The improvement of a regional climate model by coupling a land surface model with eco-physiological processes: A case study in 1998

Li Dan · Fuqiang Cao · Rong Gao

Abstract The Atmospheric-Vegetation Interaction Model (AVIM) is coupled with a Regional Integrated Environment Modeling System (RIEMS) to improve the regional simulation of climate variables. A case study in 1998 is implemented to study the improvement mechanism through land-air interaction in East Asia, especially in Asian summer monsoon regions. The coupled model reduces the warming bias in July in East China through the surface heat fluxes changes. Compared to the original model of RIEMS, the strong precipitation of eastern China in July is weakened by coupling of the interactive vegetation. The surface heat flux in uncoupled model is remarkably overestimated in these regions, and the enhanced heating from land surface, particularly with latent heat flux in July, will produce the overestimated temperature and precipitation in East China. Through coupling AVIM with RIEMS, the simulated area-averaged latent heat flux of two key regions decreases (e.g. from 132.36 to 103.13 W/m^2 over the region 1 between 105–125°E and 20–40°N) in July, which makes the overestimated temperature and precipitation declined, respectively.

1 Introduction

The region of East Asia approximately one-third global population is markedly affected by monsoonal climate (Hsu et al. 2012), which brings cold-dry weather in winter and warm-wet weather in summer. This East Asian monsoon region (EAMR) also demonstrates the strong and complicated interaction between atmosphere and biosphere due to two reasons (Fu et al. 2002): (1) the large variability of monsoon climate and weather will influence the vegetation growth and distribution; and, (2) the affected vegetation variation can simultaneously produce feedback and influence atmospheric change.

L. Dan (✉) · F. Cao
Key Laboratory of Regional Climate-Environment for Temperate East Asia, Institute of Atmospheric Physics, Chinese Academy of Sciences, Beijing 100029, China
e-mail: danli@tea.ac.cn

R. Gao
National Climate Center, China Meteorological Administration, Beijing 100081, China

In the past decade, there are studies on the interaction between climate and vegetation at the global (Foley et al. 1998; Cox et al. 2000; Dan et al. 2005a) and regional scale (Lu et al. 2001; Chen and Xie 2012). Even some are conducted in monsoon regions, e.g. the afforestation and deforestation experiment using ECHAM-JSBACH coupled model (Dallmeyer and Claussen 2011), the double CO_2 effect in MM5 (Chen et al. 2004) and the crop growth effect in RegCM3 (Chen and Xie 2012) in EAMR. The high soil moisture during summer monsoon through vegetation evapotranspiration can trigger intensified precipitation (Dan et al. 2005b). The strongest climate-vegetation biophysical effect on precipitation is in the monsoon region and the surface latent heat flux plays an important role for East Asian monsoon change (Xue et al. 2010). However, few studies focus on the regional-scale interaction between vegetation and atmosphere in EAMR. This study aims at exploring how the representation of the vegetation-related feedback mechanism in a coupled model can improve the performance of the regional climate model, in particular, by incorporating a land surface model with eco-physiological processes.

For regional-scale modeling, case studies are commonly used to highlight the regional spatiotemporal feature (Pitman and Narisma 2005; Crétat et al. 2011). The year 1998 has a typical weather event with a large summer flood in the Yangtze River Valley over EAMR (Huang et al. 1998; Tao et al. 1998). The land-air interaction contributed greatly to this large flood (Wang and Qian 2001; Dan et al. 2005b) and thus this year is appropriate for the case study of exploring the interactive atmosphere and vegetation in the regional model.

The structure of the paper is described as follows. Section 2 introduces the coupled model, observed atmospheric data, reanalysis of surface heat fluxes and NPP data. Section 3 presents the simulated results over East Asia. Section 4 concludes the findings and presents discussion of possible mechanism for the reduced bias.

2 Model and data

Both the Regional Integrated Environment Modeling System (RIEMS) and Atmospheric-Vegetation Interaction Model (AVIM) are developed by the Institute of Atmospheric Physics, Chinese Academy of Sciences. The regional climate model RIEMS has been designed within the framework of general monsoon systems (Fu 1995) since 2000 (Fu et al. 2000). RIEMS has shown good performance in simulating temperature, precipitation and atmospheric circulation in the Regional Climate Model Intercomparison Project for Asia (Fu et al. 2005). The present version 2.0 of RIEMS developed since 2007 with non-hydrostatic dynamics (Zhao et al. 2009; Zhao 2013) is used here to couple the land surface model (LSM) of AVIM.

AVIM is one of the earliest models to consider the terrestrial ecological processes in climate change modeling (Ji 1995; Dan et al. 2005a). The model has one canopy layer and ten uneven soil layers, and the physical and chemical boundary conditions in the deepest soil layer are assumed constants. The energy, momentum, and water exchange between land and air is linked with vegetation growth processes and terrestrial ecosystem carbon cycles (Dan et al. 2007). The land cover data was derived from Dorman and Sellers (1989) with modifications for China according to the China Vegetation Map (Dan et al. 2005a). The initial values by spin-up were taken from the climatological averages of the global coupled models (Dan et al. 2007).

AVIM has captured the terrestrial carbon cycle variable, net primary production (NPP), in historical and future carbon cycles of China (He et al. 2005; Huang et al. 2006), in the response to climate change of semi-arid regions (Ji et al. 2005; Lu and Ji 2006) and in the biosphere-atmospheric interaction of the global coupled models (Dan et al. 2007). AVIM also participates in the Ecosystem Model-Data Intercomparison (EMDI) organized by IGBP project on Global

Analysis, Interpretation and Modeling (GAIM). The intercomparison result is released by IGBP GAIM newsletter in the figure "EMDI Initial Results: 11 models and field NPP data at 87 sites and AVIM is the leftmost model, which is detailed at the following website: http://gaim.unh.edu/Structure/Intercomparison/EMDI/phaseIIinfo/ESA_EMDI_p2.ppt. By coupling AVIM with RIEMS, (hereafter AVIM-RIEMS) the interactive vegetation is introduced into the regional climate model.

The domain spanning between 70–140°E and 10–60°N includes the whole East Asia for RIEMS and AVIM-RIEMS (Fig.1). Here we will focus on the spatiotemporal pattern highlighted over China. Two representative regions for EAMR have been picked out to analyze the interaction between atmosphere and vegetation. We use 2.5° gridded NCEP-DOE Reanalysis 2 as the forcing data to drive REIMS and the coupled model. The boundary condition is updated very 6 h. The time step is 160 s and the integration runs from 1st July 1997 to 31th December 1998. The output data of RIEMS and AVIM-RIEMS is 60 km at spatial resolution in Lambert projection format. The observed temperature and precipitation is taken from the Climatic Research Unit (CRU), University of East Anglia with 0.5° gridded data (New et al. 1999). The 2.5° by 2.5°surface heat flux reanalysis of 40-year European Centre for Medium-Range Weather Forecasts (ECMWF) Reanalysis (ERA40, Simmons and Gibson 2000) is adopted to evaluate the simulated surface heat flux. To compare the simulated NPP, the data at half degree resolution from two biogeochemical models, Carnegie Ames Stanford Approach (CASA, Potter 1999 and 2003) and the Global Production Efficiency Model (GloPEM, Prince and Small 2003) are used in this study. CASA and GloPEM are two representative satellite-based models and they are driven by NOAA/AVHRR data (Dan et al. 2007).
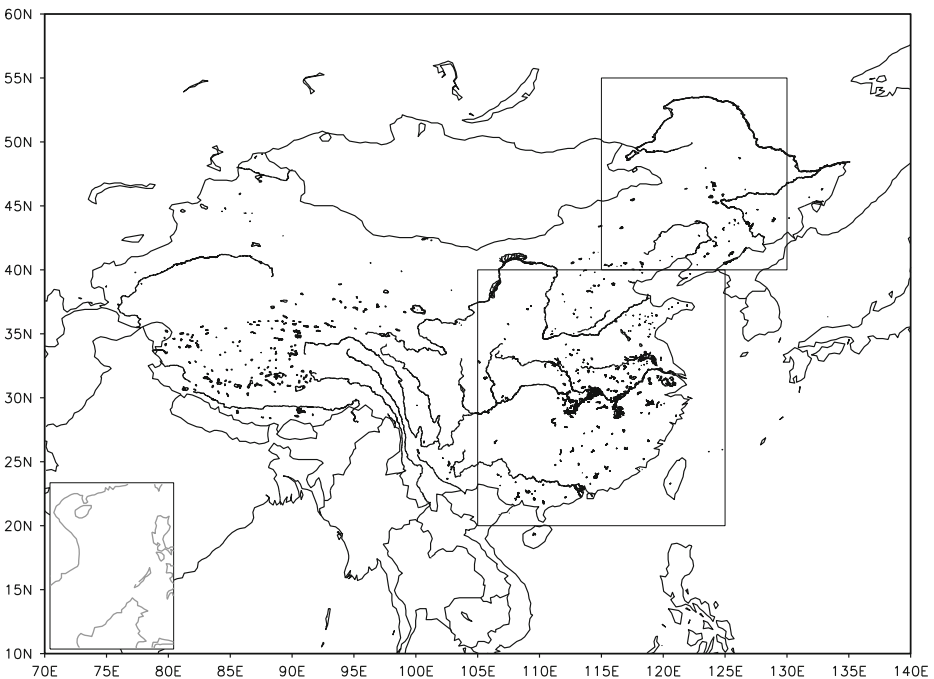

Fig. 1 The domain and two representative regions (indicated by the two rectangles as region 1 for East China and regions 2 for Northeast China) of the coupled model AVIM-RIEMS

3 Results

3.1 The atmospheric simulations of surface air temperature, precipitation and specific humidity

Figure 2 presents the surface air temperature (SAT) simulated by RIEMS and AVIM-RIEMS in January and July of 1998. Compared to the observed SAT of CRU (Fig. 2e and f), the
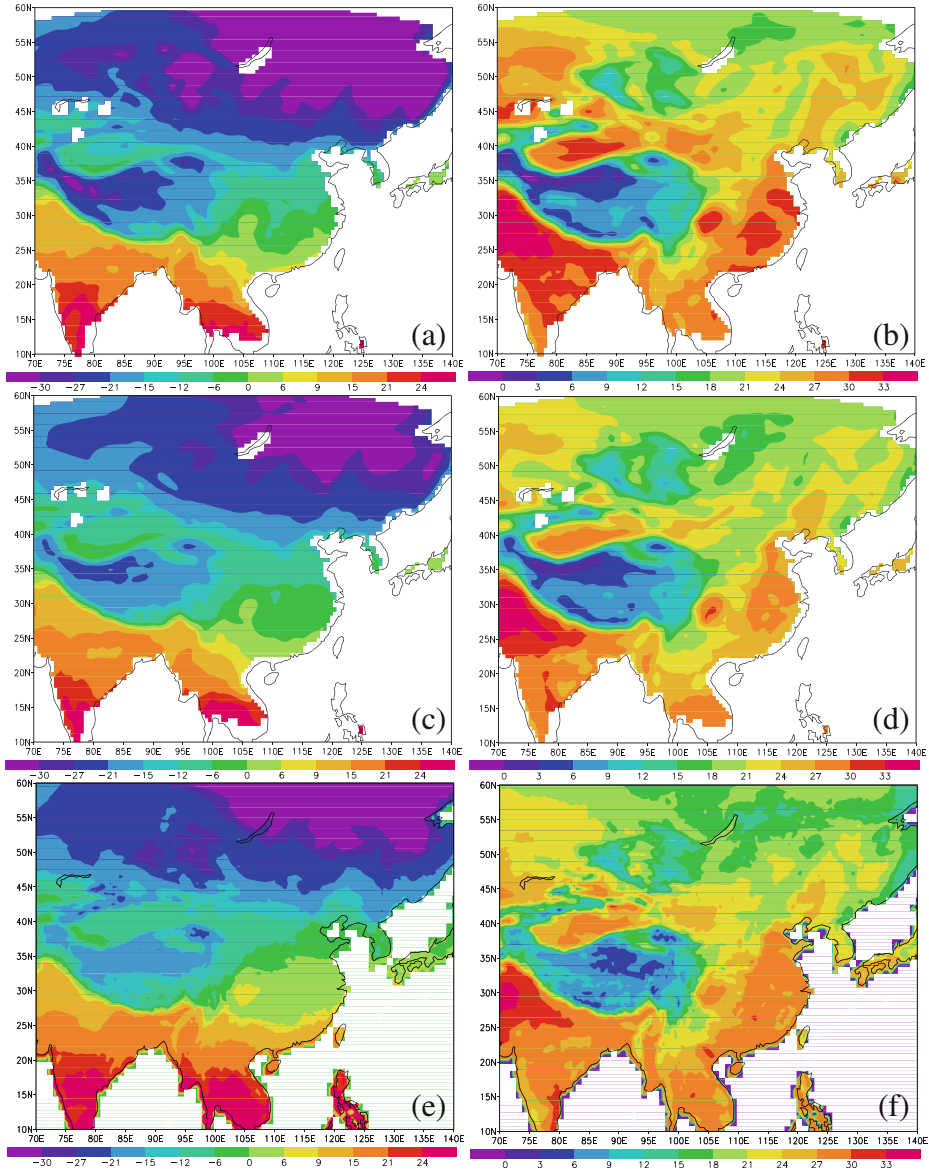
Fig. 2 The simulated and observed surface air temperature (SAT), units: °C. **a** SAT from RIEMS in January, **b** SAT from RIEMS in July; **c** SAT from AVIM-RIEMS in January, **d** SAT from AVIM-RIEMS in July; **e** SAT of CRU in January, **f** SAT of CRU in July

simulation generally underestimates SAT over China in January, even up to 8 °C by RIEMS in Northeast China, where a slight improvement of 1-2° has been made in AVIM-RIEMS. In July, the obvious enhanced SAT due to the boreal summer is shown across the whole region with exception of the Tibetan Plateau and reflects the remarkable seasonal change of EAMR. Compared to the observation of 27–30 °C in eastern China, SAT of RIEMS exhibits a strong warming center here (Fig. 2b), where the high SAT is weakened in AVIM-RIEMS (Fig. 2d) and SAT of the coupled model agrees well with CRU data. A slightly overestimated SAT also appears in Northeast China and is improved in AVIM-RIEMS. So the two regions (Fig. 1) are key regions in representing EAMR. The improved mechanism lies in the atmosphere-biosphere interaction of AVIM-RIEMS, which will use some energy and water for carbon storage during photosynthesis (Dan and Ji 2007). However, the coupled model underestimates SAT in July south of 25°N in Southeast China, which demonstrates the dominant vegetation type of broadleaf trees with ground cover should be classified further in this region as based on our previous experiment (Dan et al. 2005a).

Figure 3 shows the simulated precipitation of RIEMS and AVIM-RIEMS and observed precipitation in 1998. Less precipitation distributes in East Asia in January, and the rain belt is mainly located in South China, which extends more westward in models in contrast with CRU data. In July, large precipitation occurs in EAMR, however, the precipitation is too strong in eastern China by RIEMS (Fig. 3b). This result is improved to a degree in the coupled model (Fig. 3d), although its precipitation intensity is still higher than the observed data (Fig. 3f). The reason for this improvement is the weakened surface latent heat flux of the coupled model, which will be discussed in section 4.

Figure 4 shows the near-surface specific humidity at 1000 hPa (SPH) in 1998. In January, the SPH above 0.006 kg/kg is mainly located to south of 30°N. In July, SPH in East Asia is more than 0.01 kg/kg, whereas the simulated SPH in RIEMS is remarkably intensified with the value above 0.02 kg/kg over land along Bay of Bengal (from eastern India to Bangladesh and western Southeast Asia) and in East China (Fig. 4b). This strong SPH belt can be attributed to the large surface latent heat flux presented in the next section. Compared to ERA40 reanalysis (Fig. 4f), the overestimated SPH decreases in AVIM-RIEMS (Fig. 4d), especially along the land of Bay of Bengal, which is closer to the ERA40 data. But the SPH of the coupled model in East China is 0.002 kg/kg lower than ERA40, and the reason is needed to explore in future.

3.2 The terrestrial simulations of surface heat flux, net primary production and water use efficiency

Figure 5 presents the surface sensible heat flux (SH) over East Asia in 1998. SH more than 20 W/m^2 in January mainly distributes to south 30°N and the zero isoline indicating the equal temperature between land and air extends to around 45°N. The simulated SH is lower in northern Asia, e.g. the maximum of 20 W/m^2 underestimate in Northeast China, where the coupled model has slight higher SH than RIEMS. In July, the SH is positive in the whole East Asia, and the obviously seasonal change in contrast with January shows in northwestern China, e.g. the maximum 20 W/m^2 in January and 120 W/m^2 in July. The higher SH belt up to 160 W/m^2 can be found in RIEMS, whereas the coupled model shows the maximum of 100 W/m^2 and slightly lower than ERA40 data. The southwest-northeast gradient of this belt is reasonable in northwestern China, and the quasi west-east distribution of ERA40 seems not real, which is similar to the previous data of ECMWF 15 Years Reanalysis (Dan et al. 2005a). The simulated SH in eastern China is also overestimated in RIEMS and has some improvement in AVIM-RIEMS. The high SH in western India of RIEMS might be related to the lateral boundary exchange and would not affect greatly this study.
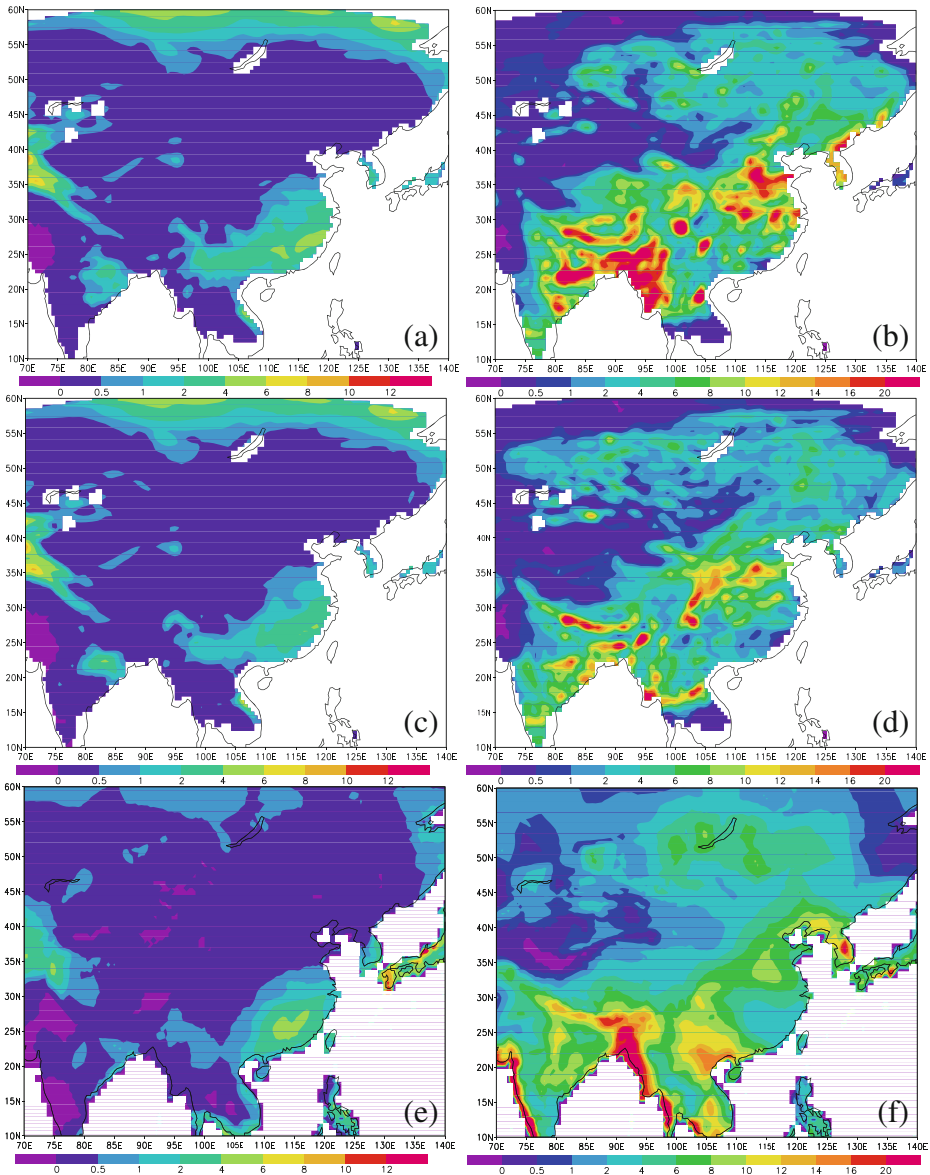
Fig. 3 The simulated and observed precipitation (PRE), units: mm/day. **a** PRE from RIEMS in January, **b** PRE from RIEMS in July; **c** PRE from AVIM-RIEMS in January, **d** PRE from AVIM-RIEMS in July; **e** PRE of CRU in January, **f** PRE of CRU in July

The distribution of surface latent heat flux (LH) of 1998 is shown in Fig. 6. LH above 10 W/m^2 in January mainly extends to south of 30°N, which reveals the major water flux in boreal winter. However, the moisture increases sharply in EAMR, which is closely related to the summer monsoon bringing much heat and moisture. The LH in East China of RIEMS (Fig. 6b) shows the too strong heating center up to 160 W/m^2 between 20 and 40°N in contrast to maximum below 140 W/m^2 and values mainly lower than 120 W/m^2 of ERA40 reanalysis
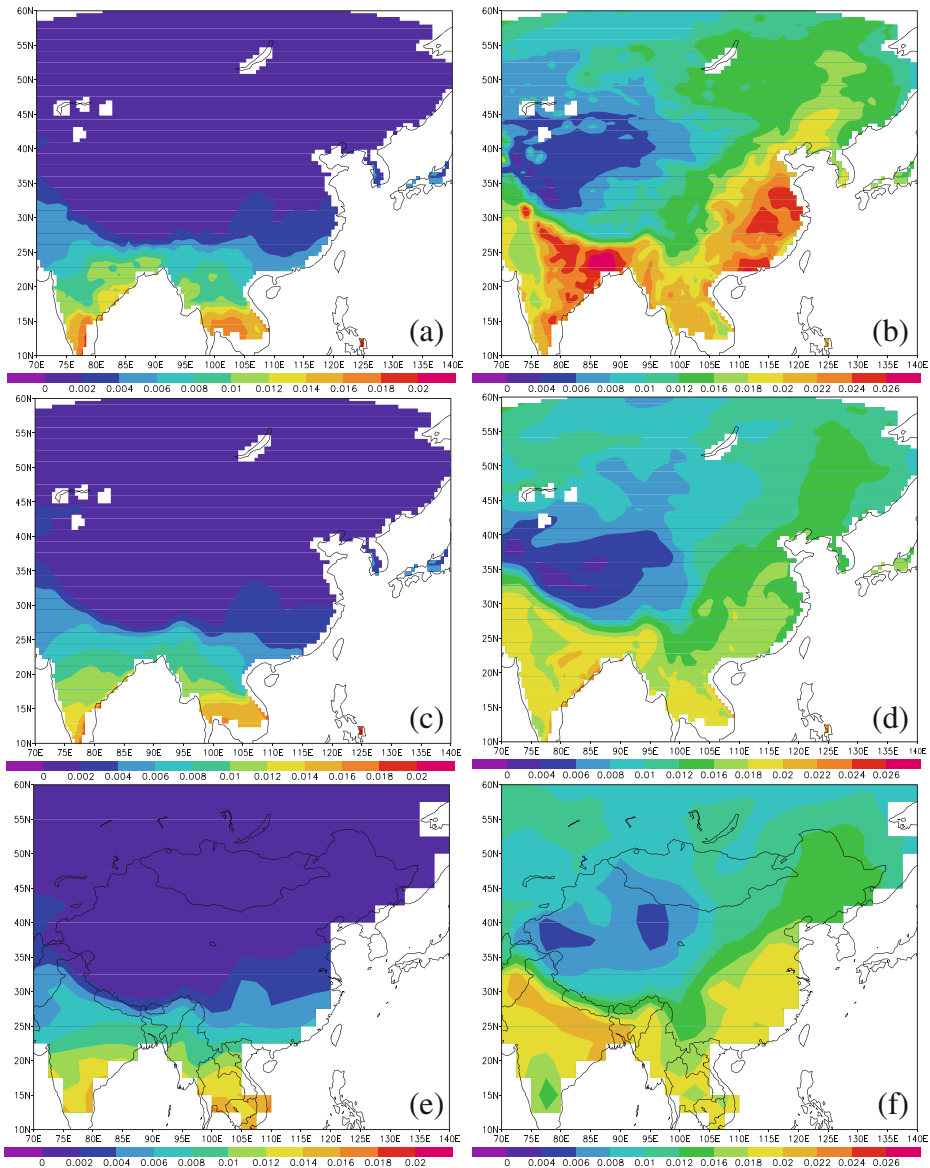
Fig. 4 The simulated specific humidity (SPH) and reanalysis data at 1000 hPa, units: kg/kg. **a** SPH from RIEMS in January, **b** SPH from RIEMS in July; **c** SPH from AVIM-RIEMS in January, **d** SPH from AVIM-RIEMS in July; **e** SPH of ERA40 reanalysis in January, **f** SPH of ERA40 reanalysis in July

(Fig. 6f). The strong surface heating is weakened below 140 W/m^2 in AVIM-RIEMS (Fig. 6d) in this region. The reason of the high LH by RIEMS is the fixed vegetation with higher soil moisture (Figures not shown here), which will provide continuous water evaporating from ground at monthly timescale. In AVIM-RIEMS, the interactive vegetation can suppress partly the excessive water evaporation by using some soil water through root to leaf in photosynthesis to produce dry matter, and the mechanism and process of water usage can be found in the equations 4,6,7,8a and 8c of Dan and Ji (2007).
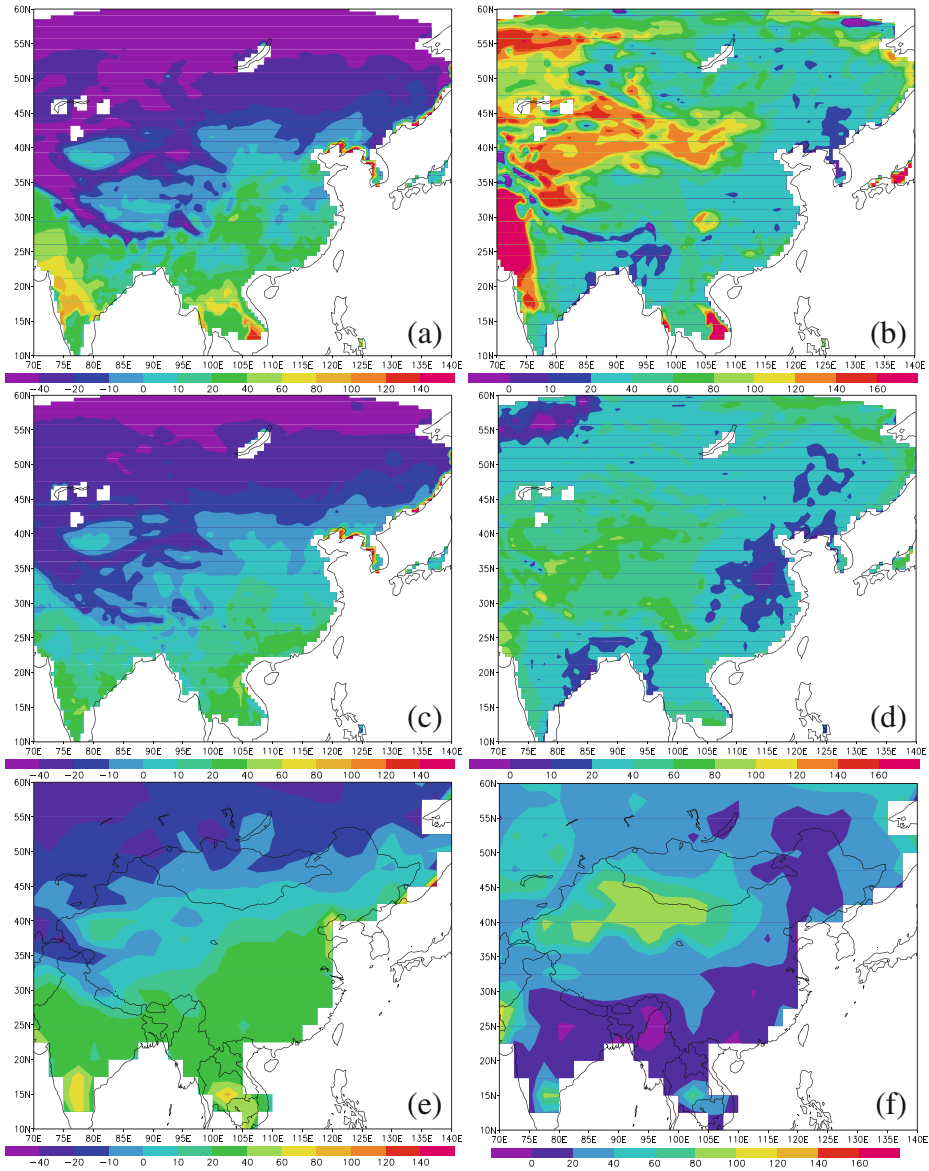
Fig. 5 The simulated sensible heat flux (SH) and reanalysis data, units: W/m^2. **a** SH from RIEMS in January, **b** SH from RIEMS in July; **c** SH from AVIM-RIEMS in January, **d** SH from AVIM-RIEMS in July; **e** SH of ERA40 reanalysis in January, **f** SH of ERA40 reanalysis in July

Figure 7 shows the annual mean NPP of 1998 from three models. NPP is one key variables of carbon cycle to fix atmospheric carbon as biomass (Zhao and Running 2010), which equals to the gross primary production (GPP) minus the carbon loss through vegetation respiration (Dan and Ji 2007). This variable is the net accumulation of photosynthetically fixed carbon from vegetation utilizing the sunlight, water and carbon dioxide to produce carbohydrate, which represents major carbon flux exchange between vegetation and atmosphere. Due to the lack of observation data of at regional scale, NPP data in 1998 from CASA (Fig. 7b) and
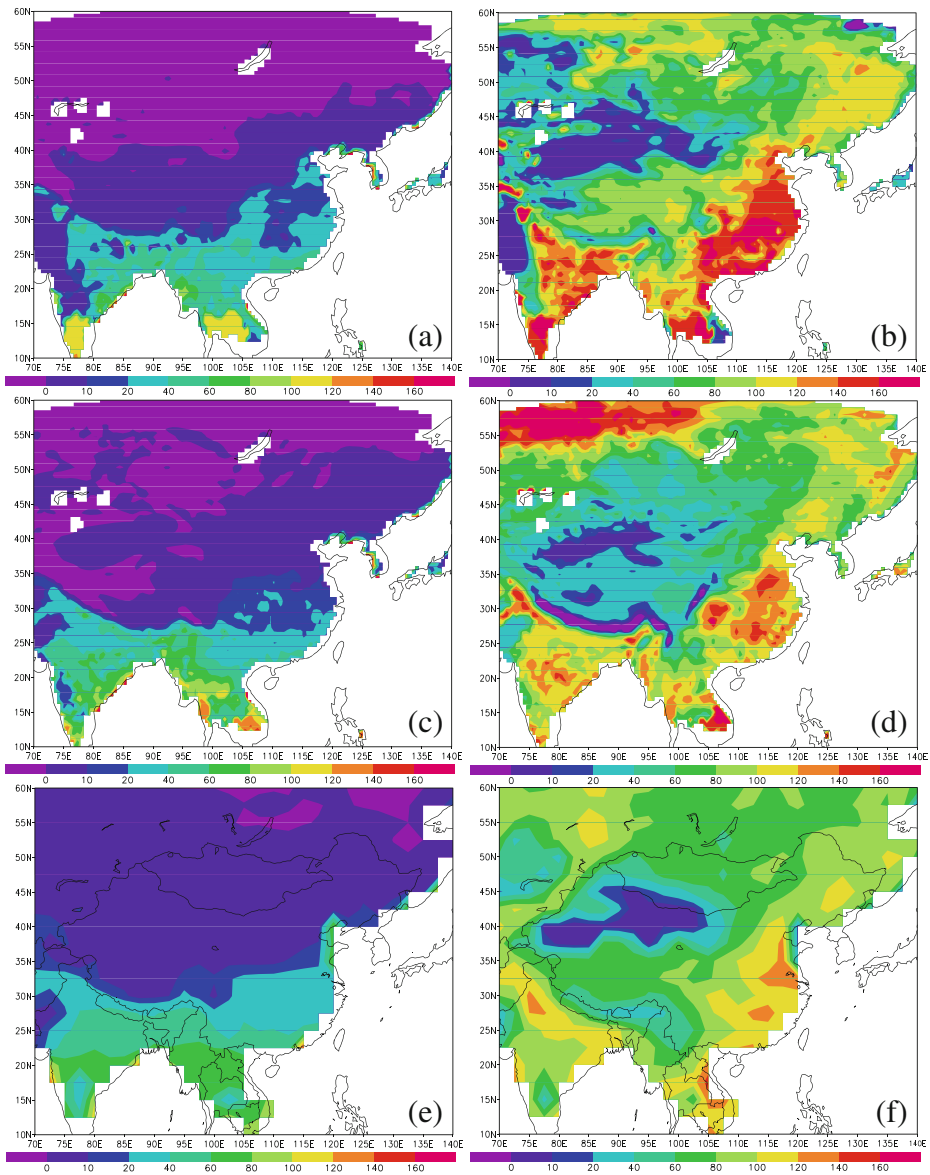
Fig. 6 The simulated latent heat flux (LH) and reanalysis data, units: W/m². **a** LH from RIEMS in January, **b** LH from RIEMS in July; **c** LH from AVIM-RIEMS in January, **d** LH from AVIM-RIEMS in July; **e** LH of ERA40 reanalysis in January, **f** LH of ERA40 reanalysis in July

GloPEM model (Fig. 7c,d) are used to test the simulation of the coupled model. The largest NPP of AVIM-RIEMS above 1000 gCm^{-2} year^{-1} mainly distributes in Southeast Asia (Fig. 7a), and the gradient decrease of 1000 to 400 gCm^{-2} year^{-1} from south to north occurs in East China. The original NPP of GloPEM is generally higher (Fig. 7c) in contrast with other models. Fortunately, the new calculated NPP in 1998 (Fig. 7d) by Cao et al. (2005) using AVHRR land data and observational climate to drive the GloPEM model has been proved to be closer to real NPP in EAMR. If the NPP of Cao et al. (2005) is selected as the benchmark,

the CASA NPP seems to underestimate NPP in East China, especially in South China. The coupled model shows the reasonable pattern, but it also underestimates the NPP in the middle and lower reaches of Yangtze River Valley centered on 30°N (See Fig. 1 for the location), which can be attributed to the lower summer carbon accumulation of AVIM-RIEMS.

3.3 Regional mean simulations averaged over two representative subregions

To investigate the regional mean atmospheric and terrestrial simulations, the area averaged values of the two key regions in EAMR are shown in Tables 1 and 2. For region 1 depicted by lower rectangle in Fig. 1, the simulated temperature in AVIM-RIEMS shows the improvement in January and July in contrast with RIEMS and CRU data. The coupled model adjusts the underestimate in January and overestimate in July by RIEMS, which shows the effect of interactive vegetation in decreasing the larger seasonal amplitude of temperature change. However, the adjustment is limited within the atmospheric dynamic framework. For example, the simulated temperature in January is much lower in RIEMS, and the interactive vegetation only increases slightly surface air temperature mainly controlled by the insufficient atmospheric radiation budget. The simulated precipitation is also affected by the interactive vegetation and closer to the observation in AVIM-RIEMS, especially in mitigating the higher value of RIEMS in July. The mechanism is that LH of the coupled model weakens the overestimated surface moisture to air, which can be shown in the near-surface specific humidity.
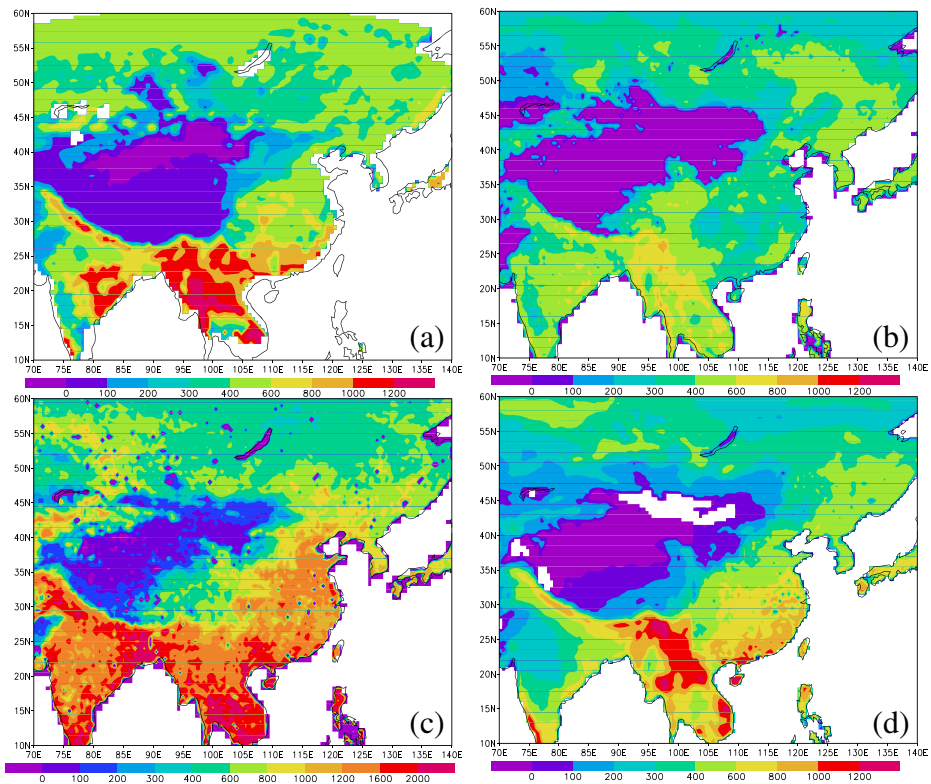
Fig. 7 The simulated annual mean net primary production (NPP) in 1998, units: $gCm^{-2} year^{-1}$. **a** NPP from AVIM-RIEMS, **b** NPP from CASA, **c** NPP from GloPEM, **d** NPP from GloPEM revised by Cao et al. (2005)

Table 1 The area-averaged values over region 1 (105–125°E, 20–40°N) in January and July. Symbol T means temperature units: °C; P means precipitation, units: mm/day; Q means specific humidity, units g/kg; S means sensible heat flux, units: W/m^2; L means latent heat flux, units: W/m^2; N means NPP, units: gCm^{-2} month^{-1}

Monthly Averages	T	P.	Q	S	L	N
AVIM-RIEMS in Jan	−4.79	1.18	2.31	12.46	18.84	4.65
RIEMS in Jan	−4.89	1.56	2.62	15.47	23.27	
Observation in Jan	3.01	1.23	4.34	28.06	38.80	
AVIM-RIEMS in July	24.53	5.28	15.31	24.45	103.13	74.87
RIEMS in July	27.50	7.81	20.99	37.23	132.36	
Observation in July	25.60	6.16	17.57	16.51	98.89	

One question may be raised that the humidity of RIEMS in January (2.62 g/kg) is lower than ERA40 of 4.34 g/kg, why the precipitation of RIEMS in January is slightly larger than CRU data. The reason can be found that the rain belt is mainly located south of 30°N in Southeast China centered 25°N (cf. Fig. 3a,c,e), whereas the specific humidity is mainly larger between 25 and 35°N for ERA40 (cf. Fig. 4a,c,e). All variables show the large seasonality between January and July in region 1, especially for NPP. The seasonal change in region 2 is very similar to region 1 and only the intensity of change is smaller in region 2, especially the small values of moisture-related variables in January.

4 Conclusions and discussion

We couple the land surface model containing interactive vegetation into RIEMS to study the possible mechanism of land-air interaction in affecting climate variables change over EAMR. The regional climate model coupled with interactive vegetation can correct the simulated bias of temperature and precipitation produced by the uncoupled model, especially in July when summer monsoon carries large amount of heat and moisture over EAMR. The mechanism mainly lies in that the surface evapotranspiration and land-air moisture flux during summer monsoon affects greatly intraseaonal change of precipitation (Xue et al. 2010) and interactive vegetation modifies the precipitation extremes through the land-air moisture feedback (Dan et al. 2005a).

The surface heating is much higher over East China in RIEMS and hence warms surface air temperature strongly, which will lead to the excessive moisture evaporating into air and thus can produce more precipitation. The soil moisture (Figures not shown here) is also overestimated in RIEMS and provides the large potential source of water for surface latent

Table 2 Same as Table 1, but for region 2 (115–130°E, 40–55°N)

Monthly Averages	T	P.	Q	S	L	N
AVIM-RIEMS in Jan	−26.39	0.22	0.41	−16.89	3.08	0
RIEMS in Jan	−30.44	0.23	0.31	−21.53	1.29	
Observation in Jan	−22.51	0.97	0.60	−0.63	5.40	
AVIM-RIEMS in July	21.35	3.26	12.27	25.16	85.93	85.66
RIEMS in July	22.60	4.80	16.10	29.47	92.69	
Observation in July	20.56	4.59	12.97	19.92	86.55	

heat flux, which causes the strong moisture feedback between land and air. By incorporating the interactive vegetation of AVIM, the strong land-air feedback is weakened due to the soil moisture consumed in the photosynthesis process for carbon production, which reduces the surface heating and the subsequent excessive moisture to atmosphere. Consequently, the coupled model AVIM-RIEMS reduces the higher bias of summer temperature and precipitation in East China.

The surface net radiation (RN) also decreases in East China (Figures not shown here) in AVIM-RIEMS due to the surface energy balance of RN=SH+LH+Q (Sellers et al. 1997), where Q is the soil heat flux with a small value. The declined RN will weaken the higher surface air temperature in RIEMS. The albedo mainly influences the surface short wave radiation and its effect is surpassed by the impact of surface heat flux on the thermal radiation. The atmosphere-vegetation interaction includes many nonlinear land-air feedbacks, and it is not a simple linear summation of individual surface processes (Xue et al. 2010). This study shows the important role of the surface heat flux on regional atmospheric change during summer monsoon in EAMR.

For dynamic vegetation-atmosphere interaction, more case studies have been carried out in Africa, e.g. MacKellar et al. (2009) using a vegetation model in Mesoscale Model (MM5) for modern atmospheric simulations. However, few cases are designed for EAMR in considering the interactive vegetation within regional climate models. This study is the case implemented in 1998, and this year is well known that soil moisture is one key factor in contributing to the summer catastrophic flood over the Yangtze River Valley (Dan et al. 2005b). The interaction between biosphere and atmosphere is of great importance to understand the mechanism of these disastrous weather events. The coupling makes it possible in the near future to consider such similar weather events. We have also simulated several cases in 1990, 1995 and 2000, and found the similar mechanism of the improvement of climate variables for AVIM-RIEMS in contrast with the regional model itself.

Overall, the result is no more than illustrative and aims at initiating the attempt to study the interaction between East Asian monsoon climate and vegetation through interactive vegetation within the framework of the regional climate model. For example, by coupling the carbon cycle into the regional model, we provide an opportunity to explore the carbon budget and carbon-atmosphere feedback over EAMR in the near future.

References

Cao MK, Prince SD, Tao B, Small J, Li KR (2005) Regional pattern and interannual variations in global terrestrial carbon uptake in response to changes in climate and atmospheric CO2. Tellus 57B:210–217

Chen F, Xie Z (2012) Effects of crop growth and development on regional climate: a case study over East Asian monsoon area. Clim Dyn 38:2291–2305. doi:10.1007/s00382-011-1125-y

Chen M, Pollard D, Barron EJ (2004) Regional climate change in East Asia simulated by an interactive atmosphere–soil–vegetation model. J Climate 17:557–572

Crétat J, Macron C, Pohl B, Richard Y (2011) Quantifying internal variability in a regional climate model: a case study for Southern Africa. Climate Dynam 37:1335–1356

Cox PM, Betts RA, Jones CD, Spall SA, Totterdell LJ (2000) Acceleration of global warming due to carbon-cycle feedbacks in a coupled climate model. Nature 408:184–187

Dallmeyer A, Claussen M (2011) The influence of land cover change in the Asian monsoon region on present-day and mid-Holocene climate. Biogeosciences 8:1499–1519

Dan L, Ji JJ, Li YP (2005a) Climatic and biological simulations in a two-way coupled atmosphere-biosphere model (CABM). Glob Planet Chang 47:153–169

Dan L, Ji JJ, Zhang PQ (2005b) The soil moisture of China in a high resolution climate-vegetation model. Adv Atmos Sci 22:720–729

Dan L, Ji JJ (2007) The surface energy, water, carbon flux and their intercorrelated seasonality in a global climate-vegetation coupled model. Tellus B 59:425–438. doi:10.1111/j.1600-0889.2007.00274.x

Dan L, Ji JJ, He Y (2007) Use of ISLSCP II data to intercompare and validate the terrestrial net primary production in a land surface model coupled to a general circulation model. J Geophys Res 112:D02S90. doi:10.1029/2006JD007721

Dorman JL, Sellers PJ (1989) A global climatology of albedo, roughness length and stomatal resistance for atmospheric general circulation models as represented by the Simple Biosphere Model (SiB). J Appl Meteorol 28:833–855

Foley JA, Levis S, Prentice IC, Pollard D, Thompson SL (1998) Coupling dynamical models of climate and vegetation. Glob Chang Biol 4:561–579

Fu CB (1995) Monsoon-driven ecosystem: Concept and some preliminary evidences, in Proceedings of the Second International Study Conference on GEWEX in Asia and GAME, Pattaya, Thailand, 6th -10th March, 68–70

Fu CB, Wei HL, Qian Y (2000) Documentation on regional integrated environmental model system (RIEMS version 1). TEACOM Science Reports START Regional Committee for Temperate East Asia, TSR

Fu CB, Wen G, Xie L, Zhao MS, Yuan HL (2002) The diagnosis and simulation studies on climate and ecosystem interactions in East Asia monsoon region. J Nanjing Univ Nat Sci 38:281–294 (in Chinese)

Fu CB, Wang SY, Xiong Z et al (2005) Regional climate model inter-comparison project for Asia. Bull Am Meteorol Soc 86:257–266

He Y, Dan L, Dong WJ, Ji JJ, Qin DH (2005) The terrestrial NPP simulations in China since Last Glacial Maximum. Chinese Science Bulletin 50:2074–2079

Hsu P, Li T, Luo JJ, Murakami H, Kitoh A, Zhao M (2012) Increase of global monsoon area and precipitation under global warming: A robust signal? Geophys Res Lett 39, L06701. doi:10.1029/2012GL051037

Huang RH, Xu YH, Wang PF, Zhou LT (1998) The features of the catastrophic flood over the changjiang river basin during the summer of 1998 and cause exploration. Clim Environ Res 3:300–313 (in Chinese)

Huang M, Ji JJ, Cao MK, Li KR (2006) Modeling study of vegetation shoot and root biomass in China. Acta Ecologica Sinica 26:4156-4163 (in Chinese)

Ji JJ (1995) A climate-vegetation interaction model: simulating physical and biological processes at the surface. J Biogeogr 22:445–451

Ji JJ, Liu Q, Li YP (2005) Modeling studies of response mechanism of steppe productivity to climate change in middle latitude semiarid regions in China. Acta Meteorologica Sinica 63:257–266 (in Chinese)

Lu LX, Pielke SRRA, Liston GE, Parton WJ, Ojima D, Hartaman M (2001) Implementation of a two-way interactive atmosphere and ecological model and its application to the central united states. J Climate 14: 900–919

Lu JH, Ji JJ (2006) A simulation and mechanism analysis of long-term variations at land surface over arid/semi-arid area in north China. J Geophyls Res 111, D09306. doi:10.1029/2005JD006252

MacKellar NC, Tadross MA, Hewitson BC (2009) Effects of vegetation map change in MM5 simulations of southern Africa's summer climate. Int J Climatol 29:885–898. doi:10.1002/joc.1754

New M, Hulme M, Jones P (1999) Representing twentieth-century space-time climate variability. Part I: development of a 1961-90 mean monthly terrestrial climatology. J Climate 12:829–856

Pitman AJ, Narisma GT (2005) The role of land surface processes in regional climate change: a case study of future land cover change over South Western Australia. Meteorol Atmos Phys 89:235–249

Potter CS (1999) Terrestrial biomass and the effects of deforestation on the global carbon cycle. Bio Science 49: 769–778

Potter CS, Klooster SA, Myneni R, Genovese V, Tan PN, Kumar V (2003) Continental-scale comparisons of terrestrial carbon sinks estimated from satellite data and ecosystem modeling 1982-1998. Glob Planet Chang 39:201–213

Prince S, Small J (2003) AVHRR global production efficiency model, 1981-2000. The Global Land Cover Facility, College Park, Maryland

Sellers PJ, Dickinson RE, Randall DA, Betts AK, Hall FG, Berry JA, Collatz GJ, Denning AS, Mooney HA, Nobre C, Sato N, Field CB, Henderson-Sellers A (1997) Modeling the exchanges of energy, water, and carbon between continents and the atmosphere. Science 275:502–509. doi:10.1126/science.275.5299.502

Simmons AJ, Gibson JK (2000) The ERA-40 project plan. ERA-40 Project Report Series 1, ECMWF, Shinfield Park, Reading, United Kingdom, p 63

Tao SY, Zhang QY, Zhang SL (1998) The great floods in the Yangtze River valley in 1998. Clim Environ Res 3: 290–299 (in Chinese)

Wang SY, Qian YF (2001) Simulation to the east Asian summer monsoon precipitation in 1998. J Nanjing Inst Meteorol 24:258–264 (in Chinese)

Xue YK, De Sales F, Vasic R, Mechooso CR, Arakawa A, Prince SD (2010) Global and seasonal assessment of interactions between climate and vegetation biophysical processes: a GCM study with different land-vegetation representations. Journal of Climate 23:1411–1433

Zhao DM, Fu CB, Yan XD (2009) Testing the ability of RIEMS2.0 to simulate multi-year precipitation and air temperature in China. Chin Sci Bull 54:3101–3111

Zhao DM (2013) Performance of regional integrated environment modeling system (RIEMS) in precipitation simulations over east Asia. Clim Dyn. doi:10.1007/s00382-012-1660-1

Zhao MS, Running SW (2010) Drought-induced reduction in global terrestrial net primary production from 2000 through 2009. Science 329:940–943. doi:10.1126/science.119266